Energy Equip. Sys./ Vol. 11/No. 4/December 2023/ 455-481

ENERGY EQUIPSYS

Energy Equipment and Systems
http://energyequipsys.ut.ac.ir
www.energyequipsys.com

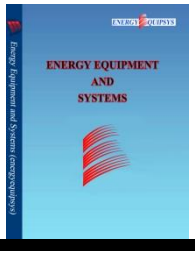

Numerical investigation of the simultaneous utilization of multiple phase change materials in the performance of thermal management system combined with heat sink

Authors

Babak Hadidi [a]
Farzad Veysi [a*]

[a] Department of Mechanical Engineering, Faculty of Engineering, Razi University, Kermanshah, Iran

Article history:

Received : 21 May 2023
Accepted :4 September 2023

ABSTRACT

Thermal management systems using phase change materials (PCMs) can improve heat absorption and increase safe operating times. However, limited research has explored combining multiple PCMs within a system. This study investigates the thermal performance of a two-dimensional heat sink with varied PCM configurations. Simulations tested RT-54, CaCl2.6H2O, anfigd n-Eicosane arranged in different ways at 5 W and 7.5 W. Key results show CaCl2.6H2O with n-Eicosane increased the time to reach 40°C by 186% compared to CaCl2.6H2O alone at 5 W. Pairing CaCl2.6H2O and RT-54 improved time to 40°C by 425%. Increased power amplified these effects. The density and latent heat fusion of PCMs were critical factors. This demonstrates combining certain PCMs extends safe operating times more than using a single material. These optimal configurations can guide thermal management system design for electronics and other applications.

Keywords: Thermal Management, Heat Sink, Phase Change Material, Numerical Simulation.

1. Introduction

With the proliferation of portable, compact and powerful electronics, effective thermal management has become imperative yet remains a significant challenge. Failure to regulate operating temperatures can lead to decreased performance, component damage, and reduced device lifetimes. As such, researchers are actively investigating novel cooling methods to meet the stringent thermal requirements of modern electronics. One emerging approach is utilizing phase change materials (PCMs) for their high energy storage density and ability to absorb substantial amounts of heat during phase transitions. However, PCM integration faces limitations like poor thermal conductivity and rapid post-melting temperature spikes that must be overcome to fully exploit their advantages. Various methods, including natural convection[1, 2], forced convection[3-5], radiative convection[6], heat pipe[7-10], boiling/ immersion [11, 12], spray cooling[13, 14], and nanofluids[15-20], have been proposed to address this issue. Among these, natural and forced convection techniques have garnered the most interest[21]. due to their high energy storage capacity, phase change materials (PCMs) have been utilized in a range of

* Corresponding author: Farzad Veysi
Department of Mechanical Engineering, Faculty of Engineering, Razi University, Kermanshah, Iran
Email: veysi_farzad@yahoo.com

applications, such as photovoltaic[22-24], buildings[25], heat exchangers[26-28], and desalination[29]. However, their low conductivity poses a significant challenge, and various methods have been suggested to improve it[30-38]. One such method involves combining PCMs with a heat sink [39, 40], temporarily maintaining a lower heat sink temperature as the PCM absorbs a substantial amount of heat during the phase change[41, 42]. Yet, once the PCM melts, the temperature rises sharply[22]. Consequently, using PCM in a heat sink is only beneficial if the applied power duration is shorter than the melting time[41], and the input power must be removed before the PCM melting is complete, presenting a challenge for this method. Table 1 presents a summary of the studies conducted in this field and their differences with the present work [43-70].

In this study, a two-dimensional simulation analysis was conducted to examine the impact of using multiple phase change materials, individually and simultaneously, on the performance of a finned heat sink with a PCM structure. Three distinct materials n-Eicosane, RT-54, and $CaCl_2.6H_2O$ were simulated in combined and individual arrangements within a heat sink under constant input power across six different configurations. Two power levels, 5 W and 7.5 W, were utilized as heat sources. The volumetric fraction of the phase change material was set to 1, while the volumetric fraction of fins in the heat sink was considered to be 9%. As the simultaneous use of phase change materials has not been extensively studied, this research focuses on the effects of employing different phase change materials, both separately and in combination, on the operating duration at a safe thermal temperature, the average system temperature, and the maximum system temperature.

2. Physical and geometrical properties

2.1 Physical structure

The geometry under investigation is a two-dimensional heat sink designed to dissipate heat using multiple fins. Each fin has a thickness of 2 millimeters, and the volumetric fraction of fins in the heat sink is considered to be 9%. Recent experimental studies by Arshad et al. [68, 70, 71]and Ashraf et al.[72, 73] have reported that a finned heat sink with a 9% volumetric fraction offers optimal thermal performance for passive thermal management in portable electronic devices. Equation 1 is used to determine the volumetric fraction of the fins in the heat sink:

$$\Psi = \frac{V_{fin}}{V_{HS}} \quad (1)$$

In this equation, V_{fin} represents the volume of the fins, while V_{HS} denotes the volume of the heat sink without fins. The area surrounding the fins is filled with phase change material. Table 2 presents the thermophysical properties of the heat sink and phase change materials:

A heater with 5 and 7.5 W powers is used to simulate an electronic processor. The heat sink's surroundings are considered to be insulated. Figure 1 displays the full dimensions and specifications of the various components of the heat sink:

2.2 Governing Equation

The enthalpy-porosity method is utilized to model the phase change effect of the phase change material in the finned heat sink. Continuity, momentum, and energy equations are solved simultaneously for heat transfer modeling, with the melting/solidification model applied to the phase change issue. The governing equations for mass, momentum, and energy are as follows:

Table 1: Summarized recent studies on thermal management with PCMs and Differences with this work

ref	year	Passive/Active heat transfer	Single PCM/ multi PCMs	Experimental /Numerical	Topic	Differences
Present work	2023	passive	Single and multi PCMs	Numerical	• The impact of employing one or multiple phase change materials (PCMs) on thermal management • Using different layouts of PCM • The effect of increasing the input power on the operating time of the system at thermal safe temperature • Investigating the thermal behavior of PCMs under different input powers	-
Lamba, R., et al [43]	2023	Passive	Single PCM	Numerical	• Investigating integrated heat sink, PCM, and radiative cooling for PV temperature regulation • Testing 8 combinations of HS, PCM, and RC for PV performance improvement	No multi PCMs
Hu, X., et al [44]	2023	Passive	Single PCM	Numerical	• Investigating thermal performance and optimization of metal foam PCM-based heat sinks for thermal management of electronics • Analyzing different design parameters: PCM types (RT31, RT42, RT55), metal foam porosities (85%, 90%, 95%), materials	No multi PCMs
Elshaer, A.M., et al [45]	2023	Passive	Single PCM	Numerical	• Investigating PCM-integrated thermal control devices (TCDs) for satellite electronics thermal management • Adopting RT35 organic PCM in TCD for small satellite subsystem under zero gravity • Using various pin fin geometries (square, circular, triangular, cross, I, V shapes) to improve PCM thermal conductivity	No multi PCMs
Balakrishnan, R., et al.[46]	2023	Passive	Single PCM	Experimental	• Investigating heat sink with PCM and silicon carbide nanoparticles for thermal management of electronics • Mixing varying silicon carbide nanoparticle compositions (1-3 wt%) in paraffin wax PCM	No multi PCMs
Tharwan, M.Y., et al.[47]	2022	Passive	Single PCM	Experimental	• Improved heat sink cooling through the use of a PCM	No multi PCMs
Sheikh, Y., M., et al.[48]	2022	Passive	Single PCM	Experimental	• Investigating effects of PCM filling height and copper foam pore density on cooling performance of a bio-PCM composite heat sink • Testing three PCM filling height ratios (1.0, 1.3, 1.6) and three copper foam pore densities (35, 80, 95 pores per inch (PPI))	No multi PCMs

Rehman, T.-u., et al.[49]	2022	Passive	Single PCM	Experimental	• Investigating thermal management using nickel foam and RT-44HC paraffin PCM heat sinks for electronics • Using nickel foam for high heat transfer area with minimal reduction in PCM latent heat	No multi PCMs
Manoj Kumar, P., et al [50]	2022	Passive	Single PCM	Experimental	• Investigating thermal performance impacts of PCM and nano-enhanced PCM (NIPCM) in heat sinks for electronics	No multi PCMs
Mahmud, H., et al [51]	2022	Passive	Single PCM	Numerical	• Investigating melting of paraffin wax PCMs for thermal control in microgravity spacecraft • Conducting 2D simulations of 12 arrangements of heat source-sink pairs in a square cavity • Analyzing stored energy, liquid fraction, and heat transfer characteristics	No multi PCMs
Kim, J., et al [52]	2022	Passive	Single PCM	Experimental	• Developing layer-by-layer (LbL) carbon nanotube-polyethyleneimine interfaces between PCM and heat sink	No multi PCMs
Jalil, J.M., et al [53]	2022	Passive	Single PCM	Experimental	• Investigating the effect of using phase change material (PCM) on heat sink cooling performance • Adding 2% aluminum oxide nanoparticles to PCM improves performance further	No multi PCMs
Al-Omari, S.A.B., et al.[54]	2022	Passive	Single PCM	Numerical	• Investigating a new lifted fin concept for PCM heat sinks, where fins are detached from the hot base instead of attached • Numerically analyzing thermal management of a gallium PCM heat sink with vertical plate fins lifted at different levels from the hot base	No multi PCMs The study is investigating detached/lifted fins in a PCM (gallium) heat sink, versus traditional attached fins.
Ali, H.M.[55]	2022	Passive	Single PCM	Experimental	• Investigating methods to improve thermal conductivity of phase change materials (PCMs) for thermal management • Investigating methods to improve thermal conductivity of phase change materials (PCMs) for thermal management	No multi PCMs
Wang, S., et al.[56]	2021	Passive	Single PCM	Experimental	• Investigating thermal performance of heat sinks using higher alcohol and higher alcohol/graphite foam PCMs	No multi PCMs
Sunku Prasad ., et al.[57]	2021	Active	Single PCM	Experimental	• Analyzing the impact of a PCM on the thermal performance of a heat sink in forced convection	No multi PCMs No passive cooling

Hu, X. and X. Gong [58]	2021	Passive	Single PCM	Experimental	• Using structured porous material (SPM) as a thermal conductivity enhancer (TCE) to improve heat sink performance • Testing heat sinks with SPM of different porosities (80%, 85%, 90%, 95%) • Evaluating thermal response at various heating power levels (8W, 10W, 12W)	No multi PCMs This study Provides guidance on design and application of SPM in PCM-based thermal management units
Ho, J.Y., et al.[59]	2021	Passive	Single PCM	Experimental And Numerical	• Investigating topology optimization (TO) of PCM-filled heat sinks to improve thermal performance • Numerically studying effects of heat transfer mechanisms on TO design	No multi PCMs
Dammak, K. and A. El Hami [60]	2021	Passive	Single PCM	Numerical	• Numerically studying effects of heat transfer mechanisms on TO design • Investigating thermal reliability optimization of pin fin heat sink filled with phase change material (PCM) • Using aluminum pin fins and paraffin wax PCM to study cooling performance for electronics	No multi PCMs
Taghilou, M. and E. Khavasi [61]	2020	Passive	Single PCM	Experimental And Numerical	• Investigating thermal reliability optimization of pin fin heat sink filled with phase change material (PCM) • Using aluminum pin fins and paraffin wax PCM to study cooling performance for electronics • "Optimizing the system's operating time at the optimal temperature with and without the use of a PCM	No multi PCMs The main focus was on maximizing the operation time
Motahar, S. and M. Jahangiri [62]	2020	Passive	Single PCM	Numerical	• Identifying the optimal PCM to use for thermal energy storage purposes within the temperature range of 40-80 °C • Employing a (MADM) approach to determine the most suitable PCM	No multi PCMs The main focus was on finding the best PCM with multi attribute decision making (MADM)
Gaddala, U.M. and J.K. Devanuri [63]	2020	Passive	Single PCM	Numerical	• Assessing the thermal storage potential of various PCMs by comparing their thermal conductivity • Establishing a distinct coefficient (hd) for the thermal conductivity of PCMs in heat transfer	No active cooling No multi PCMs

Debich, B., et al.[64]	2020	Passive	Single PCM	Numerical	• Investigating the impact of a constant and variable thermal load on a heat sink, both with and without PCM • Four different fin configurations were considered	No multi PCMs
Akula, R. and C. Balaji [65]	2020	Passive	Single PCM	Numerical	• Examining the influence of augmenting the thermal surface area of a heat sink integrated with a PCM on its thermal management efficacy	No multi PCMs
Kalbasi, R., et al.[66]	2019	Passive	Single PCM	Experimental And Numerical	• Determining the ideal number of fins and the appropriate volume fraction of PCM	No multi PCMs The main focus was on optimizing the number of fins and volume fraction
Usman, H., et al [67]	2018	Passive	Single PCM	Experimental	• Investigating the thermal performance of a heat sink integrated with PCM, both with and without fins • Studying the effects of different types of fins in PCM heat sink	No multi PCMs The main focus was on the effects of different forms of fin on PCM heat sink
Arshad, A., et al [68]	2018	Passive	Single PCM	Numerical	• Investigating the impact of a single fin within a square cavity • Examining the influence of fin length and cavity orientation on the process of meltdown	No multi PCMs The main focus was on fin length and direction of cavity on the meltdown process

Table 2: Thermophysical properties of phase change materials and heat sink

properties	n–Eicosane	RT-54	$CaCl_2.6H_2O$	Aluminum
Tm (K)	309.5	327.15	302.15	–
L (J/kg)	241,000	200000	170000	–
Cp (J/kg.K)	2050	2000	2230	871
ρ (kg/m3)	790	850	1710	2719
k (W/m.K)	0.23	0.2	1.088 solid 0.529 fluid	202.4

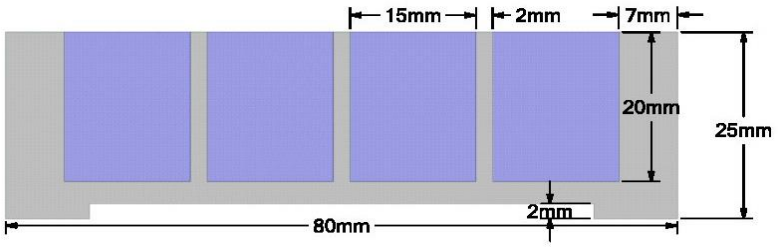

Fig.1: The dimensions of the different sections of the investigated heat sink

Mass conservation equation:

$$\frac{\partial u}{\partial x}+\frac{\partial v}{\partial y}=0 \tag{2}$$

Momentum conservation equation:

$$\rho\left(\frac{\partial u}{\partial t}+u\frac{\partial u}{\partial x}+v\frac{\partial u}{\partial y}\right) = -\frac{\delta P}{\delta x}+\mu\left(\frac{\partial^2 u}{\partial x^2}+\frac{\partial^2 u}{\partial y^2}\right)+S_u \tag{3}$$

$$\rho\left(\frac{\partial v}{\partial t}+u\frac{\partial v}{\partial x}+v\frac{\partial v}{\partial y}\right) = -\frac{\delta P}{\delta y}+\mu\left(\frac{\partial^2 v}{\partial x^2}+\frac{\partial^2 v}{\partial y^2}\right)+S_v \tag{4}$$

Energy conservation equation:

$$\rho C_P\left(\frac{\partial T}{\partial t}+u\frac{\partial T}{\partial x}+v\frac{\partial T}{\partial y}\right) = k\left(\frac{\partial^2 T}{\partial x^2}+\frac{\partial^2 T}{\partial y^2}\right)+S_h \tag{5}$$

In these equations, P represents pressure, g is gravitational acceleration, ρ is density, μ is dynamic viscosity, ρC_P is heat capacity, k is thermal conductivity, t is time, and u and v denote the velocity components in the x and y directions, respectively. The S value in the momentum equations is expressed as:

$$S=-A_m(\varphi) \tag{6}$$

Here, $A_m(\varphi)$ is the porosity function defined by Brent et al.[74], inspired by the Carman-Kozeny relation for porous media. This relation's fundamental principle is that the velocity gradually decreases from a finite velocity inside the liquid state to zero in the solid state during numerical calculations in the phase change time. Consequently, for the nth fluid cells undergoing phase change within the mushy zone, $A_m(\varphi)$ is defined as transforming the momentum equation into Carman-Kozeny equations for porous media:

$$A_m(\varphi)=-C\frac{(1-\varphi)^2}{(\varphi^3-b)} \tag{7}$$

In these calculations, $b=0.001$ is used to avoid denominator to be zero. The constant C represents the shape of the melting site, controlling the continuous fluid displacement's degree within the mushy phase change region. The value of C is set to 10^5, as recommended in numerous studies[75-77]. A mushy zone lies between two liquid fraction values of 0 and 1. The liquid fraction is defined as:

$$\varphi=\frac{\Delta H}{L} \tag{8}$$
$$=\begin{cases}0 & if\ T<T_s\\ \dfrac{T-T_s}{T_l-T_s} & if\ T_s<T<T_l\\ 1 & if\ T>T_l\end{cases}$$

The mathematical models employed in this research are detailed in the works of Niak et al.[78], Shatikian et al.[77, 79], Sahu et al.[80], and Wang and Yang[75, 76]. These papers have simulated the thermal performance of using internal fins for heat transfer. In the studies by Hosseinzadeh[81] and Fok et al.[82], a strong agreement between simulation results and experimental results has been reported. Therefore, the above method is used for simulation in this work.

3.Boundary Conditions and Initial Conditions

In this research study, boundary and initial conditions are based on the experimental works of Arshad et al. [68, 72] and Ashraf et al. [73]. A two-dimensional schematic of the physical domain employed in this research is illustrated in Fig.2. The outer boundary walls are defined as adiabatic boundary conditions. Due to the phase change phenomenon, the simulation process occurs in a transient state.

- Initial condition

At the start of the simulation, the entire thermal management system has a uniform temperature of 25 degrees Celsius, and the volumetric fraction of phase change materials is equal to zero, with all materials in the solid state.

$$t=0,\ T=T_{in},\ \varphi=0$$

4.Numerical solution

Grid and time step independence have been examined to mitigate their impact on the results. Three grids with dimensions of 3,760 cells, 15,040 cells, and 60,160 cells were studied to assess grid independence. Figure 3 displays the change in the average temperature of the heat sink over time for these three different computational grids.

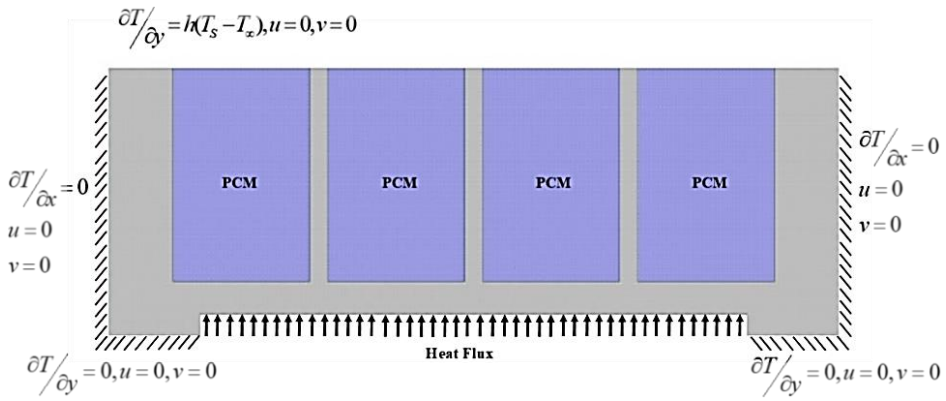

Fig.2: Boundary conditions

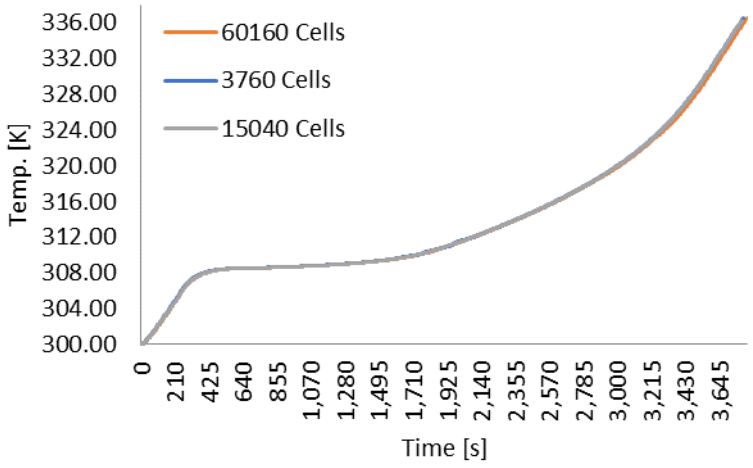

Fig. 3: Grid independence study

The melting time and average base temperature for all three grids are presented in Table 3. The results demonstrate that the maximum deviation in melting time and average heat dissipation temperature is found to be 0.02 and 0.26 percent, respectively. Three-time intervals of Δt = 0.05 s, 0.1 s, and 0.2 s were investigated, with the results shown in Fig. 4. After comparing the results, the grid with 15,040 elements and a time step of Δt = 0.1 s were selected for the simulation.

5.Validation

To validate the model and ensure the accuracy of the numerical method used, temperature and volume fractions have been compared with the results of Hosseini and colleagues[83]. Figure 5 presents the validation results, demonstrating a maximum discrepancy of 5% relative to experimental data.

Table 3: Melting Time and Average Base Temperature for Each Network

Network	Number of Nodes	Melting Temperature	Deviation Percentage	Average Heat Sink Temperature	Deviation Percentage
0.5	3760	308.4	0.02%	337.814	0.26%
0.25	15040	308.34	0.00%	338.711	0.00%
0.125	60160	308.35	0.003%	338.71	0.0003%

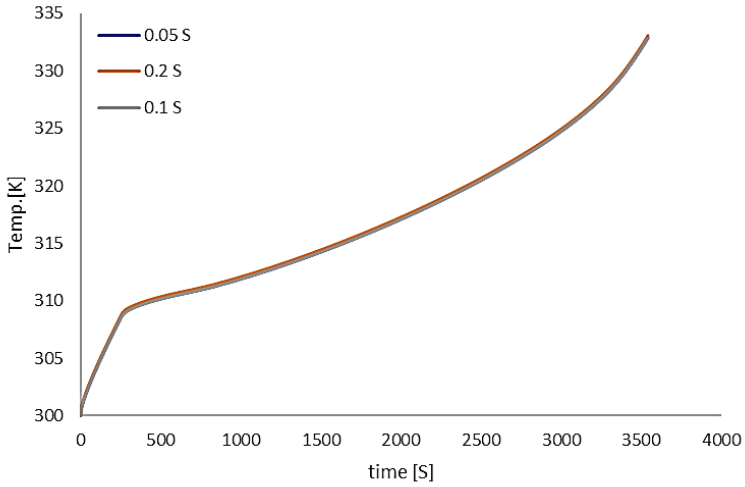

Fig.4: Time independence study

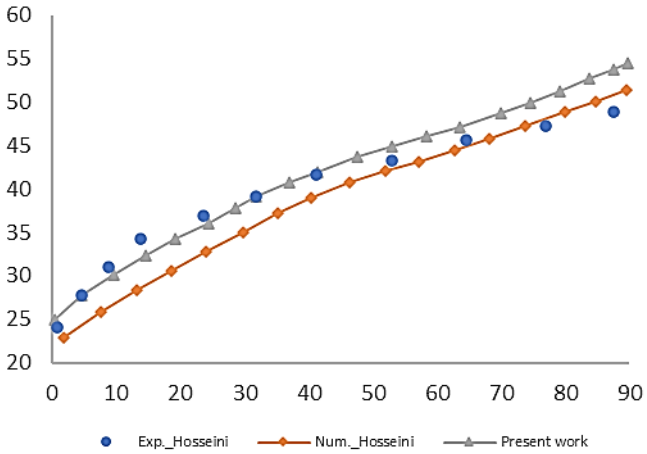

Fig.5: Validation of the numerical study

6.Results

6.1.First scenario

In the initial scenario, the heat sink's thermal performance was examined individually with each of the three materials: n-Eicosane, $CaCl_2.6H_2O$, and RT-54. Here, the heat sink was filled exclusively with one of these materials, and a simulation was conducted at two input power levels: 5 and 7.5 W.

Figures 6A and 6B illustrate the progression of maximum temperature over time for this scenario. Among the materials, $CaCl_2.6H_2O$ demonstrated the strongest resistance to a temperature increase during the melting phase. n-Eicosane also exhibited a later melting point compared to RT-54. The graph of liquid volume fraction (Figs. 7A and 7B) shows RT-54 with the most pronounced slope during the melting process. The maximum temperatures observed align with these trends: RT-54 reached the highest temperature, followed by n-Eicosane, with $CaCl_2.6H_2O$ registering the lowest. As the input power increased, the melting duration for all materials shortened, and the system's peak temperature rose.

The influence of integrating phase change material into the thermal management system is assessed based on the duration needed to reach various set point temperatures (SPTs)[84], where electronic equipment remains undamaged. Figure 8 reveals that the time for the system's temperature to meet the specified

level differs across materials and for distinct SPTs of 40, 45, and 55 degrees Celsius. At an SPT of 40 °C, $CaCl_2.6H_2O$, when powered at 5 W, takes the longest duration, approximately 3.7 times longer than n-Eicosane and 11 times longer than RT-54 (Fig.8 - A). Under the same conditions, n-Eicosane requires thrice the time of RT-54 (Fig.8 - A). When the power is increased to 7.5 W, $CaCl_2.6H_2O$'s duration extends to 10.5 times that of RT-54 and 4.2 times that of n-Eicosane (Fig.8 - A). Meanwhile, n-Eicosane's duration is 2.5 times that of RT-54 (Fig.8 - A).

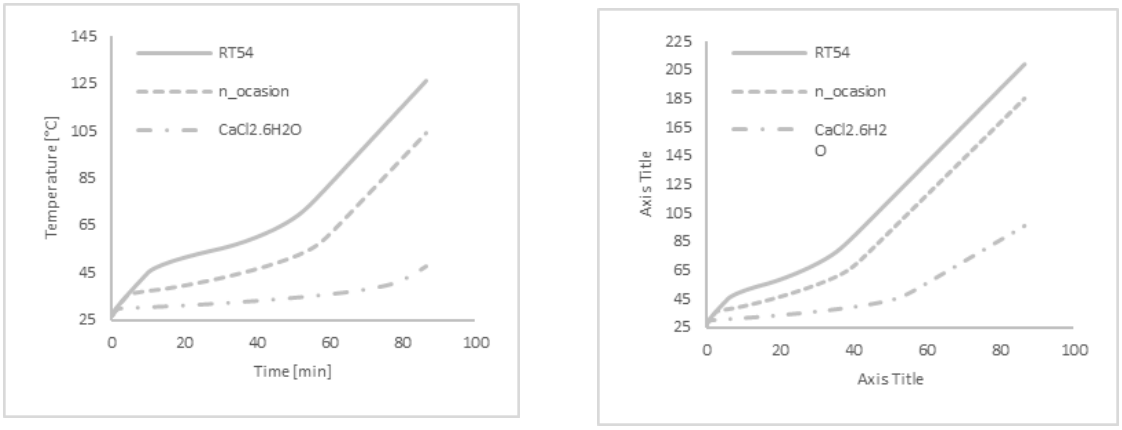

A) 5 B) 7.5

Fig.6: Temperature fluctuations for each of the three phase change materials at input power levels of 5 and 7.5 W

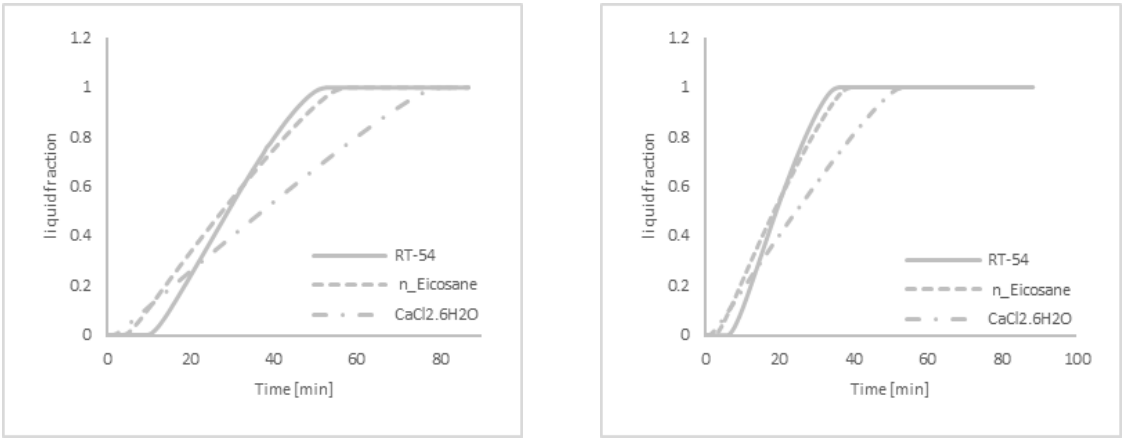

A) 5 B) 7.5

Fig. 7: Changes in liquid volume fraction for each of the three PCMs at input power levels of 5 and 7.5 W

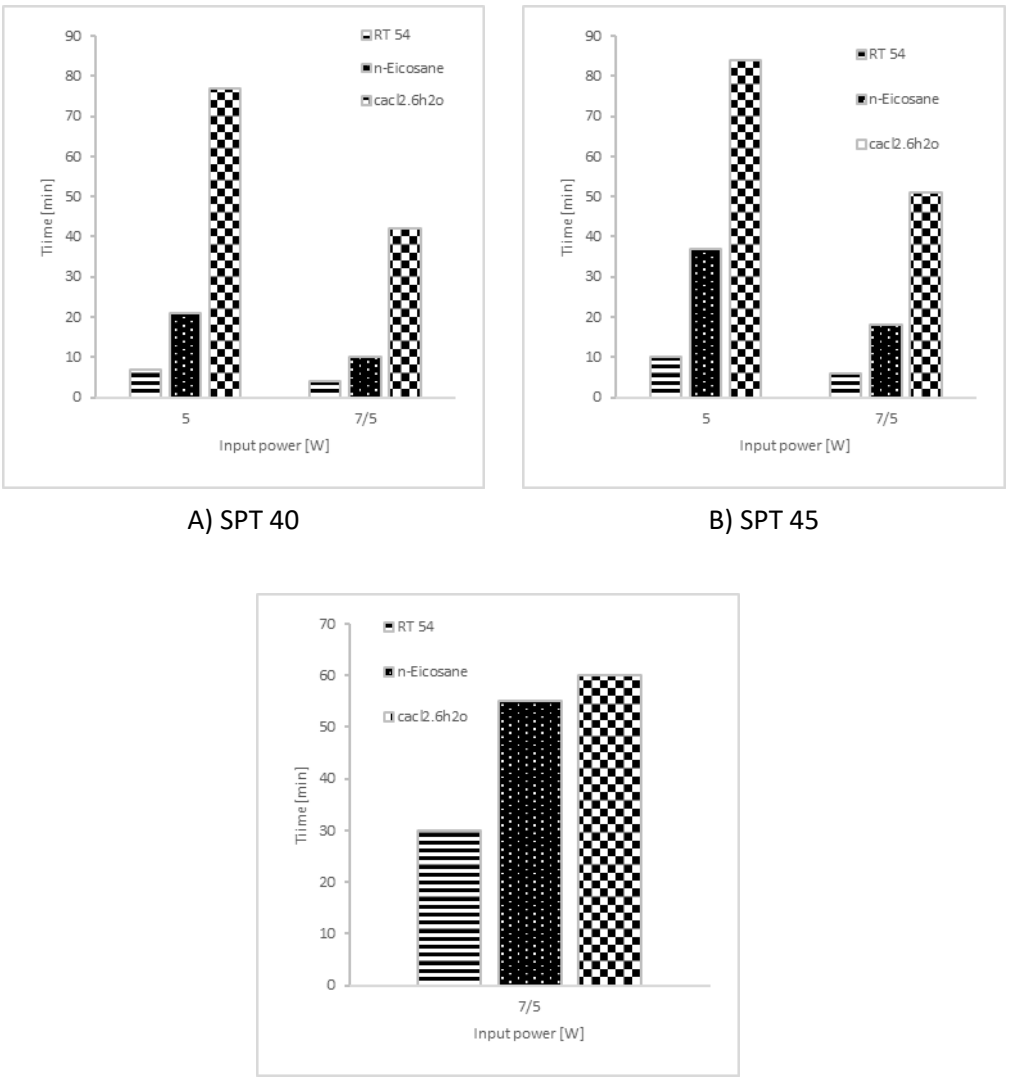

Fig.8: Conditions for different SPTs in each of the three PCMs at input powers of 5 and 7.5 W

Moving to an SPT of 45 °C, $CaCl_2.6H_2O$ takes 2.37 times the duration of n-Eicosane and 8.5 times that of RT-54 when powered at 5 W (Fig.8- B). Under these conditions, n-Eicosane's duration is 3.7 times that of RT-54. At 7.5 W, the duration for $CaCl_2.6H_2O$ increases to 8.5 times that of RT-54 and 2.8 times that of n-Eicosane (Fig.8 - B), with n-Eicosane requiring thrice the duration of RT-54.

Lastly, for an SPT of 55 °C, $CaCl_2.6H_2O$ does not reach 55 degrees at 5 W (Fig. 8 - C). However, at 7.5 W, $CaCl_2.6H_2O$'s duration is twice that of RT-54 and only 10% longer than n-Eicosane (Fig.8-C). n-Eicosane, in this instance, requires a duration 1.8 times longer than RT-54 (Fig.8 - C).

The average temperature is lowest for the scenario utilizing $CaCl_2.6H_2O$, followed by n-Eicosane, with RT-54 exhibiting the highest average temperature (Fig.9). A surge in input power increases the system's average temperature across all scenarios (Fig.9).

Figure 10 presents the contours of the liquid volume fraction at various intervals for the three materials n-Eicosane, $CaCl_2.6H_2O$, and RT-54 at 7.5 W.

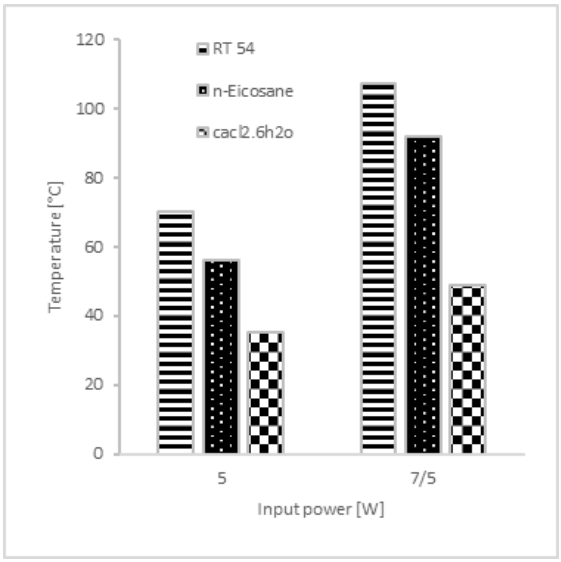

Fig.9: The thermal management system's mean temperature (in degrees Celsius) at input powers of 5 and 7.5 W.

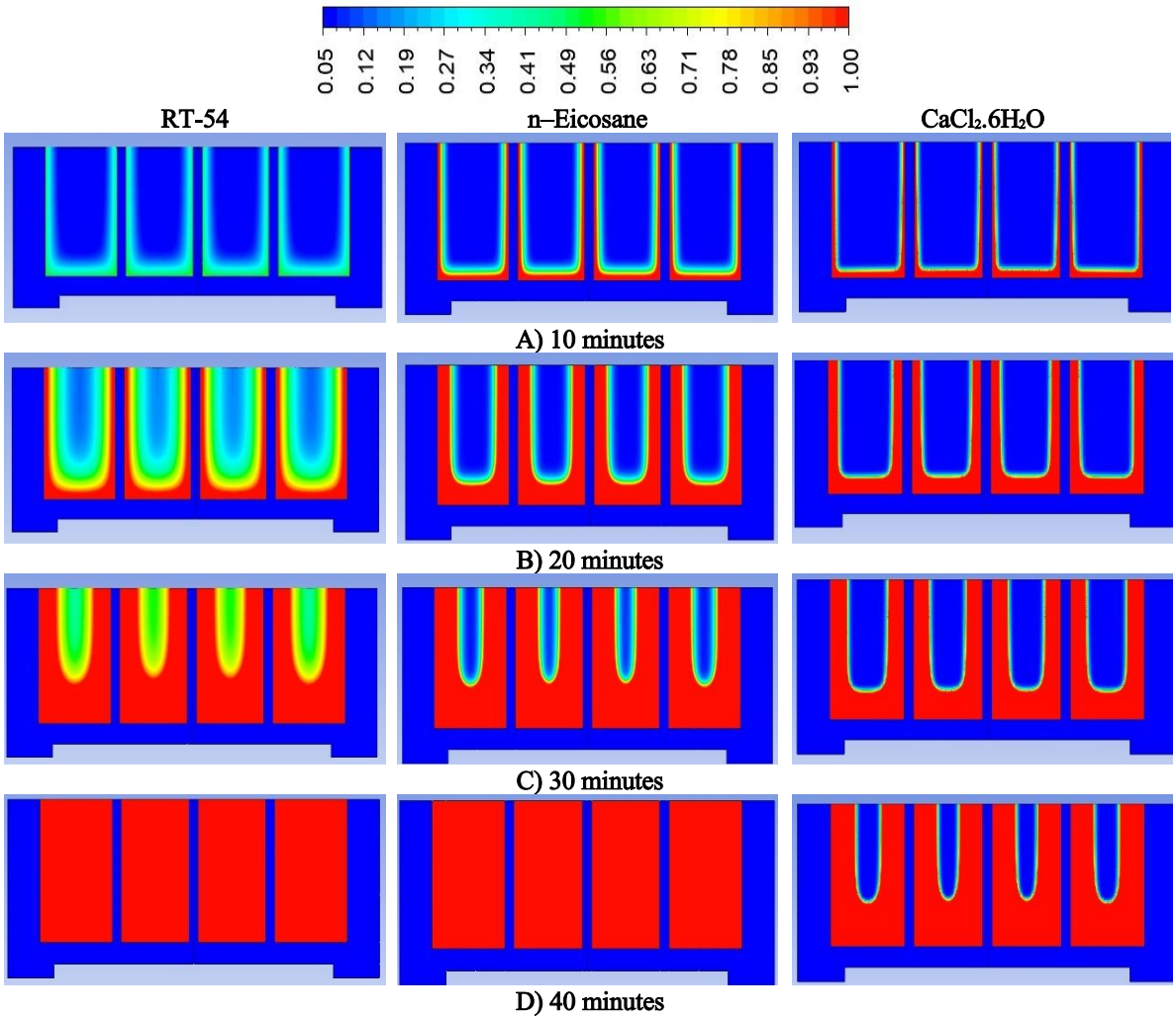

Fig. 10: Liquid volume fraction contours over time for each of the three PCMs at 7.5 W.

6.2.Second Scenario: CaCl2.6H2O and RT-54

The second scenario introduces a combination of two materials, $CaCl_2.6H_2O$ and RT-54, used as phase change materials within the heat sink. Here, RT-54 is positioned adjacent to the heat source, while $CaCl_2.6H_2O$ is situated distantly from it. Simulations were carried out for two input powers, 5 and 7.5 W.

Figures 11a and b depict the system's peak temperature fluctuation over time for this scenario. For RT-54, the temperature curve initially ascends, then descends post reaching the melting point (Fig.11-a). Following the melting phase, the temperature change slope experiences a rise. As input power is elevated to 7.5 W, the system reaches the melting temperature more rapidly, shortening the melting duration and significantly raising the maximum system temperature (Fig.11-b). For $CaCl_2.6H_2O$, the material swiftly attains the melting temperature, causing a notable decline in the temperature curve's slope. Post-melting, the slope escalates once more. As input power intensifies, melting duration lessens, and the final temperature also elevates. The presence of dual melting points is distinctly visible on the liquid volume fraction chart when both materials are employed simultaneously for both 5 W and 7.5 W inputs (Fig.12-a and b).

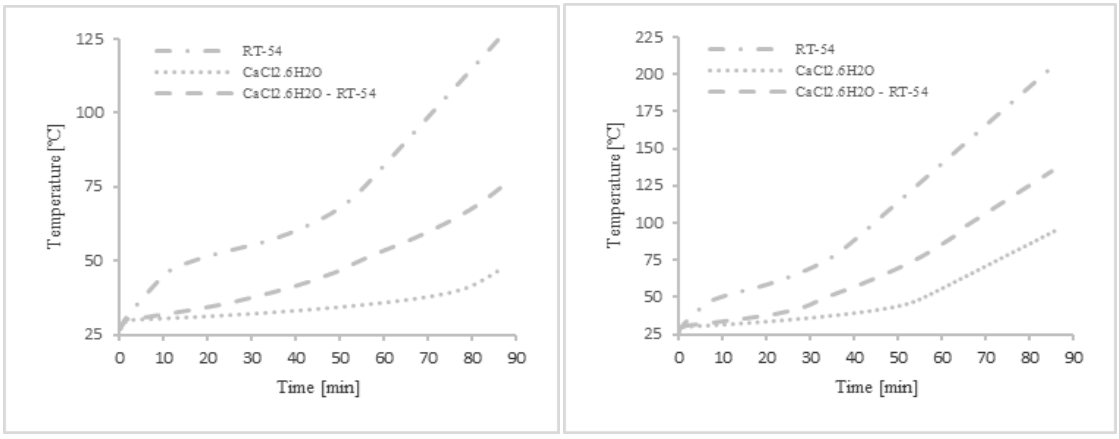

Fig.11: Temperature fluctuations for the second scenario: CaCl2.6H2O and RT-54 at input powers of 5 and 7.5 W.

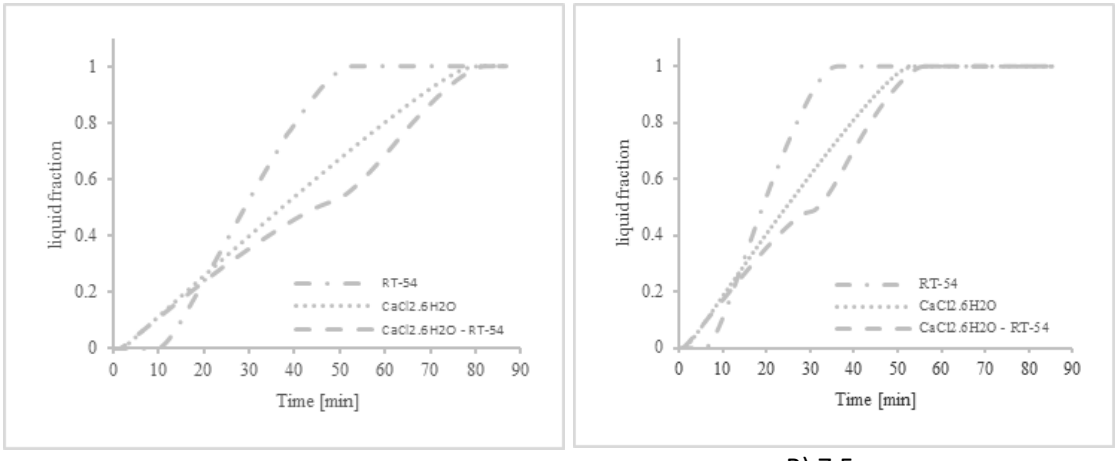

Fig.12: Alterations in liquid volume fraction for the second scenario: CaCl2.6H2O and RT-54 at 5 and 7.5 W input powers.

Figure 13 illustrates the varying durations required for the system temperature to attain specific Set Point Temperatures (SPTs) of 40, 45, and 55 degrees Celsius in different materials and their combinations. At an SPT of 40 degrees Celsius and an input power of 5 W, employing two substances simultaneously prolongs the time to reach the target temperature by 425%, while at a power of 7.5 W, this duration escalates by 525% in comparison with the RT-54 condition (Fig.13-A). Regarding an SPT of 45 degrees Celsius, the time extension is 370% at 5 W and 383% at 7.5 W relative to RT-54 (Fig.13-B). For an SPT of 55 degrees Celsius at 7.5 W, the extension is 144% (Fig.13-C).

The lowest average temperature is observed in the $CaCl_2.6H_2O$ scenario; subsequently, the combined scenario demonstrates superior performance. Increasing input power elevates the average system temperature across all cases (Fig.14).

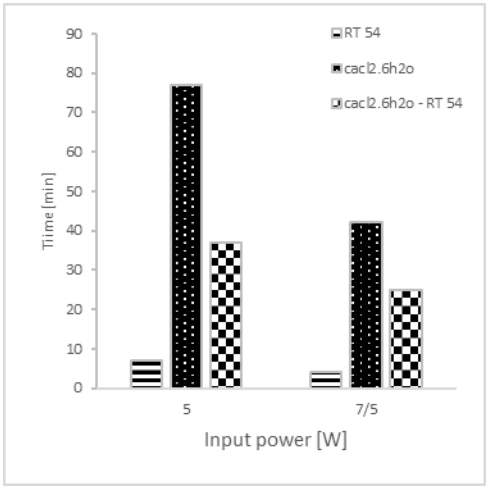

A) SPT 40

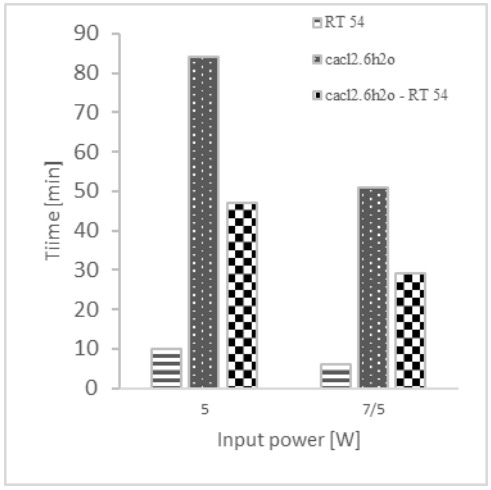

B) SPT 45

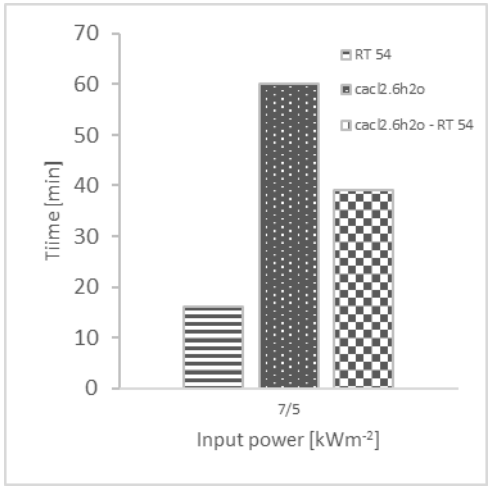

C) SPT 55

Fig.13: Set Point Temperature conditions for the second scenario of CaCl2.6H2O and RT-54 at 5 and 7.5 W input powers.

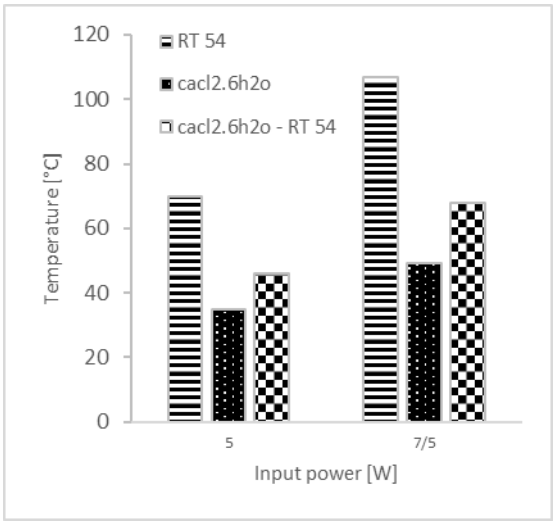

Fig.14: Average system temperature for the second scenario of CaCl2.6H2O and RT-54 at 5 and 7.5 W input powers.

Figure 15 portrays the contours of the volumetric fraction of liquid at various times across three scenarios of $CaCl_2.6H_2O$, RT-54, and the combined scenario with an input power of 7.5 W.

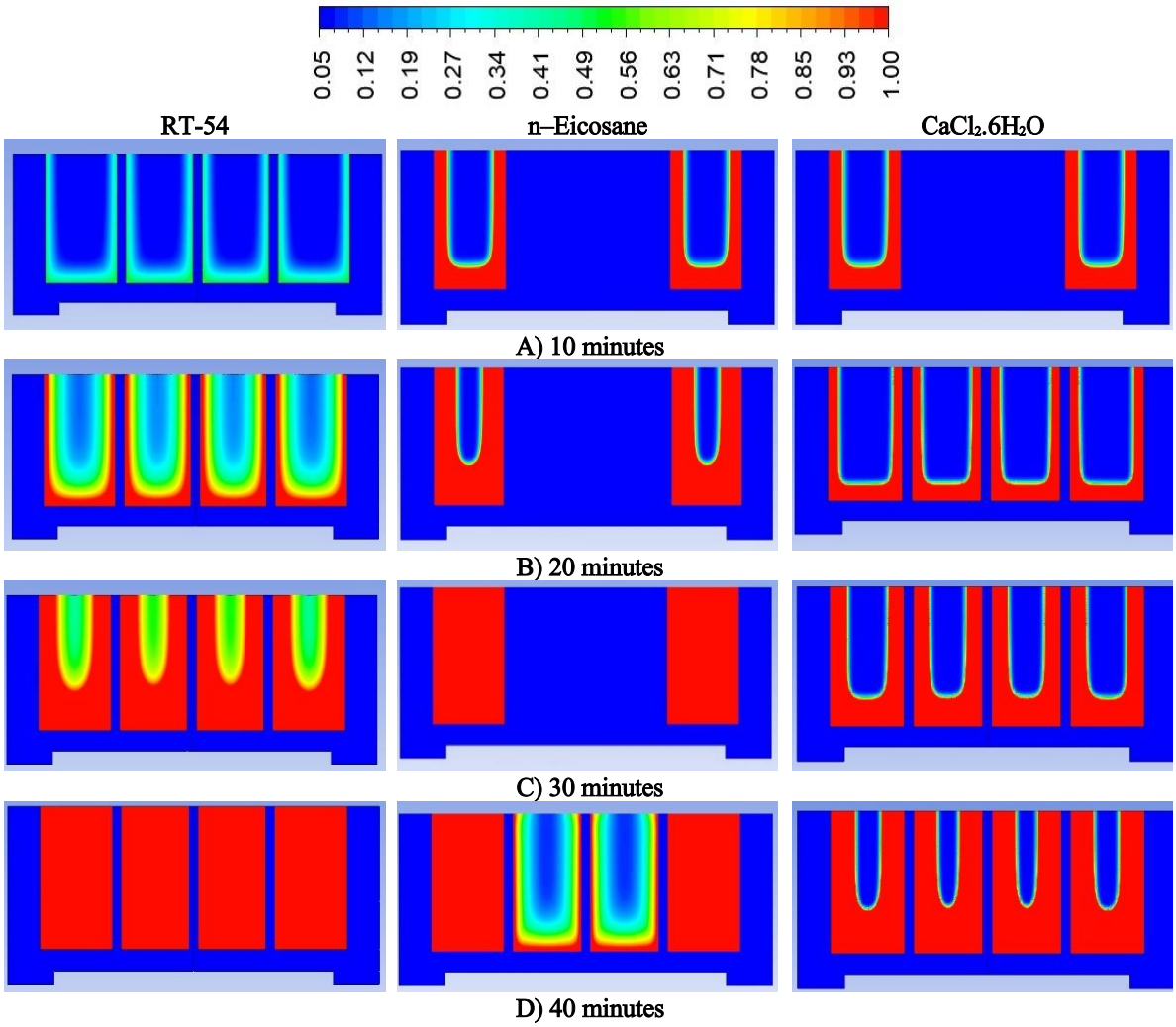

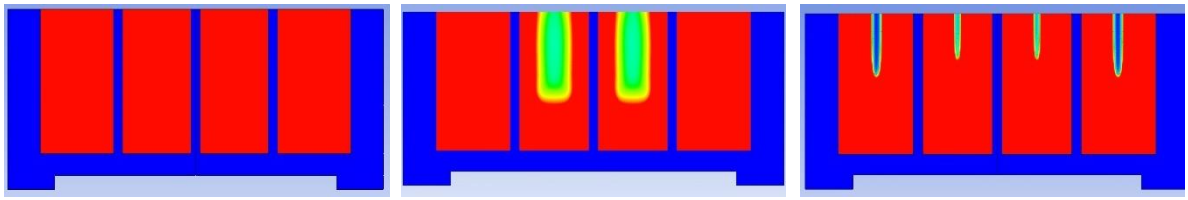

E) 50 minutes

Fig.15: Volumetric fraction of liquid at different times for the second scenario of CaCl2.6H2O and RT-54 at 7.5 W power

6.3. Third scenario: $CaCl_2.6H_2O$ and n–Eicosane

In the third scenario, two substances of $CaCl_2.6H_2O$ and n–Eicosane are used as phase-changing materials in the heat sink. In the scenario of simultaneous use of two substances, n–Eicosane is on the heat source, and $CaCl_2.6H_2O$ is far from the heat source. The simulation has been done for two input powers of 5 and 7.5 W.

Figures 16 A and B show the graph of maximum temperature changes over time for the third scenario. For n–Eicosane, the temperature graph initially increases, and after reaching the melting point, the slope of the graph decreases (Fig.16-A). After complete melting, the slope of temperature changes increases. At 7.5 W of power, the set reaches the melting temperature faster, the melting time is shorter, and the maximum system temperature is much higher than before. For $CaCl_2.6H_2O$, the substance quickly reaches the melting temperature. At the melting temperature, the slope of the temperature change graph decreases significantly. After melting, the slope of temperature changes increases again. With the increase of input power, the melting time becomes shorter, and the final temperature also increases. At 5 W power, the presence of two melting points for the scenario of simultaneous use of two substances is clearly visible on the graph of the volumetric fraction of liquid (Fig.17-A), but with an increase of power to 7.5 W, the graph becomes continuous, and it is impossible to distinguish two melting points (Fig.17-B).

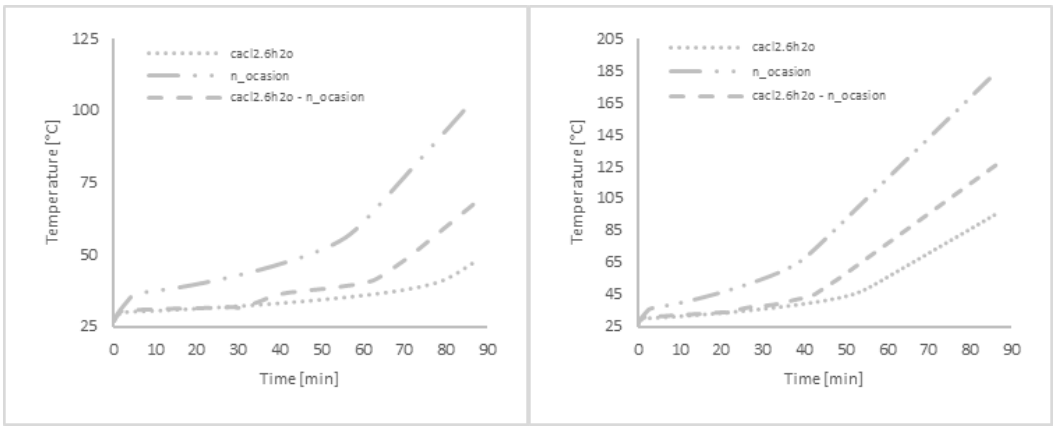

A) 5 B) 7.5

Fig.16: Temperature variations for the third scenario CaCl2.6H2O and n–Eicosane in 5 and 7.5 watt input powers

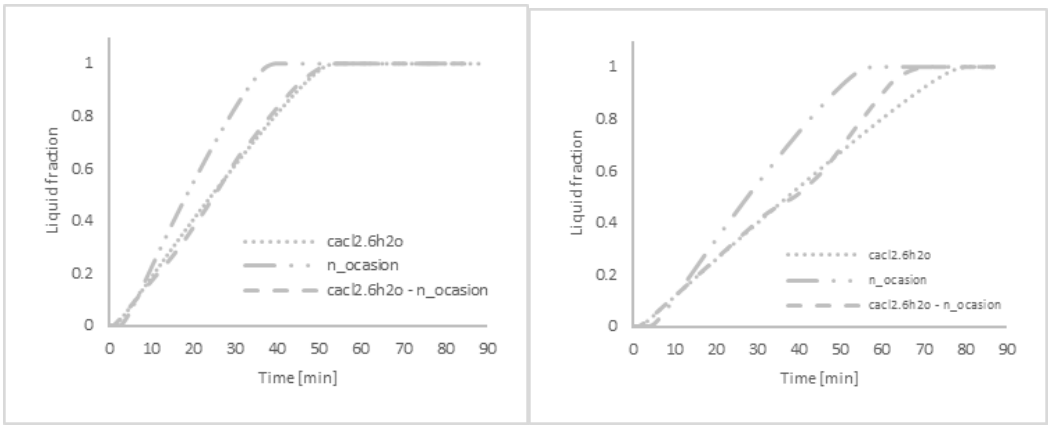

A) 5 B) 7.5

Fig.17: Changes in the volume fraction of liquid for the third scenario CaCl2.6H2O and n–Eicosane in 5 and 7.5 watt input powers

Figure 18 illustrates the variance in duration necessary for the system temperature to reach predetermined SPTs of 40, 45, and 55 degrees Celsius across different materials and their combined scenario. At an SPT of 40 degrees Celsius, employing two materials concurrently at 5 W amplifies the operating time by 186%, and at a power of 7.5 W, this extends by 250% compared to the n–Eicosane condition (Fig. 18-A). For an SPT of 45 degrees Celsius, the time increment is 81% at 5 W and 133% at 7.5 W relative to the n–Eicosane scenario (Fig.18-B). For an SPT of 55 degrees Celsius at 7.5 W, the extension is 60% (Fig.18-C).

The minimum average temperature is exhibited by the $CaCl_2.6H_2O$ condition, followed by the combined scenario with superior performance. A surge in input power prompts an elevation in the average system temperature across all scenarios (Fig.19).

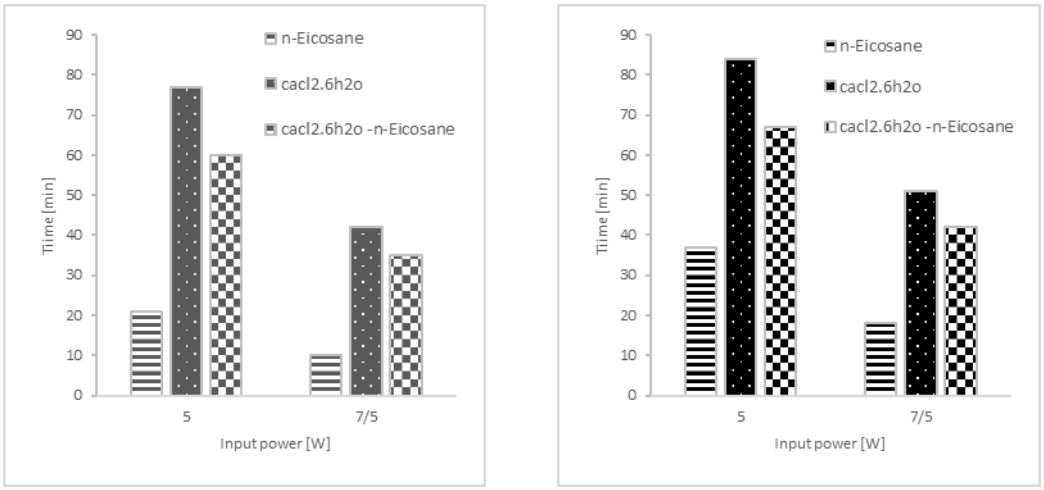

A) SPT 40 B) SPT 45

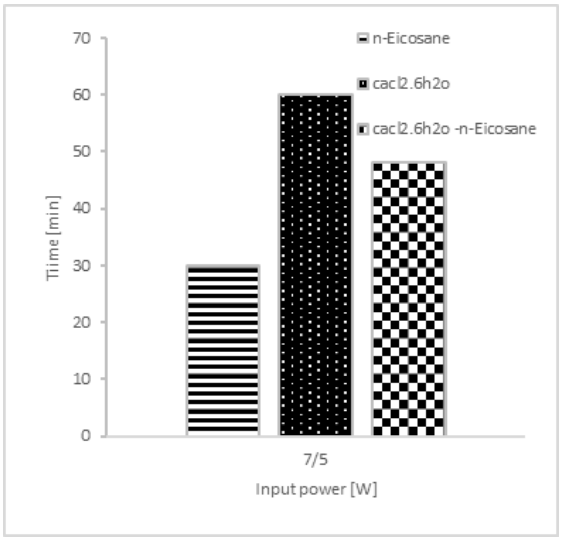

C)SPT 55

Fig.18: Set Point Temperature conditions for the third scenario involving CaCl2.6H2O and n–Eicosane at input powers of 5 and 7.5 W

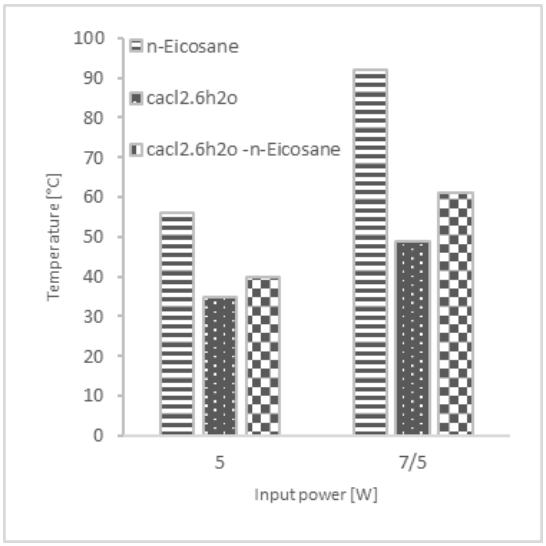

Fig.19: Average temperature of the thermal management system for the third scenario involving CaCl2.6H2O and n–Eicosane at input powers of 5 and 7.5 W.

Figure 20 presents the contours of the volumetric fraction of liquid at varying times for all three scenarios— $CaCl_2.6H_2O$, n–Eicosane, and the combined scenario—at an input power of 7.5 W.Fourth scenario: RT-54 and n–Eicosan

The fourth scenario employs RT-54 and n–Eicosane as phase change materials within the heat sink. In concurrent use of these substances, n–Eicosane is positioned near the heat source, while RT-54 is stationed farther away. Simulations were carried out for input powers of 5 and 7.5 W.

Figure 21 depicts the progression of maximum temperature changes over time for these cases. In the RT-54 scenario, the temperature curve initially ascends, and its slope reduces upon reaching the melting point (Fig.21-A). Following complete melting, the temperature change slope rises again. When the input power is amplified to 7.5 W, the system

reaches the melting temperature more swiftly, the melting duration diminishes, and the maximum system temperature significantly exceeds the previous case (Fig.21-B). In the n–Eicosane scenario, the temperature change slope decreases markedly at the melting point but, after complete melting, increases again. With increased input power, the melting duration decreases, and the final temperature also rises.

In concurrently using both materials, two distinct melting points are clearly discernible on the liquid volume fraction chart at both input powers of 5 and 7.5 W (Fig.22-A). An increase in input power heightens the liquid volume fraction chart's slope and reduces the melting time (Fig.22-B).

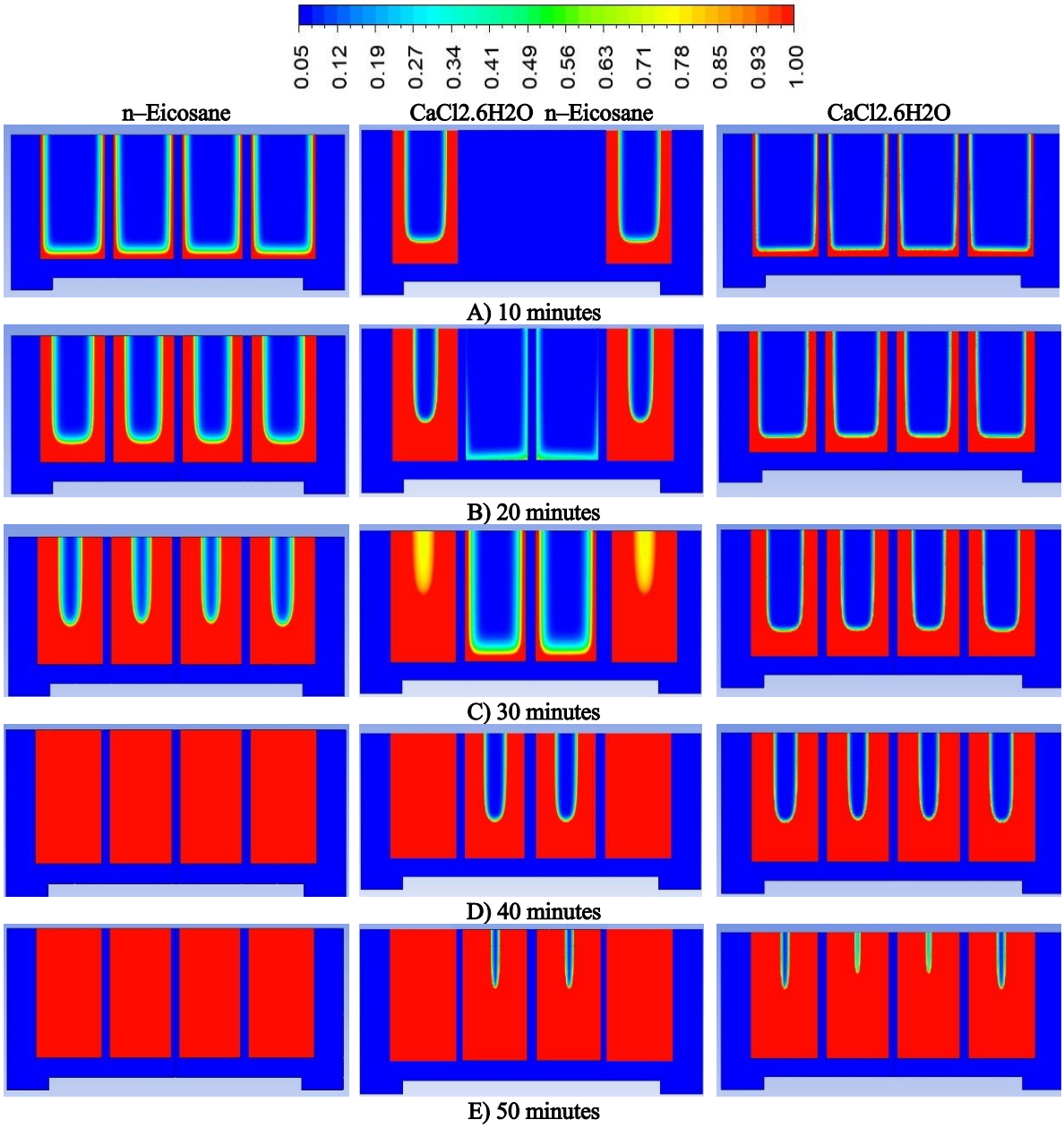

Fig.20: Volumetric fraction of liquid at different times for the third scenario involving CaCl2.6H2O and n–Eicosane at an input power of 7.5 W

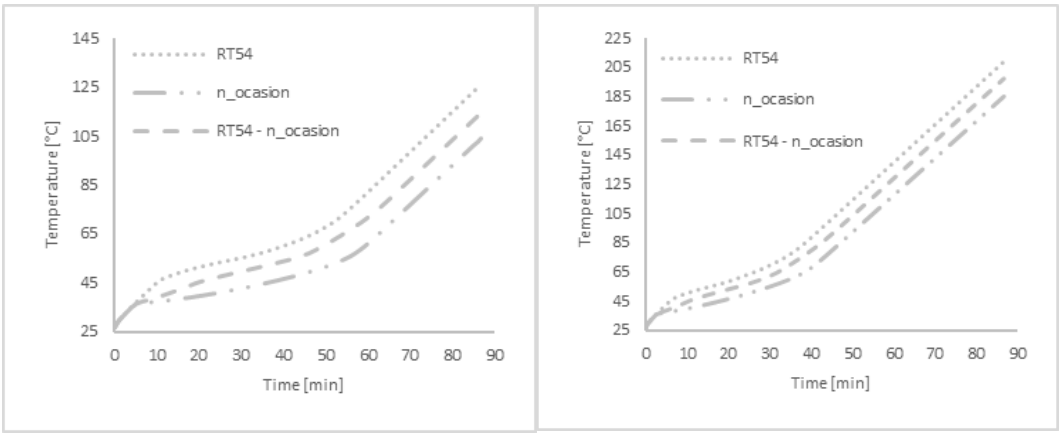

A) 5 B) 7.5

Fig.21: Temperature changes for the fourth scenario involving RT-54 and n–Eicosane at input powers of 5 and 7.5 W.

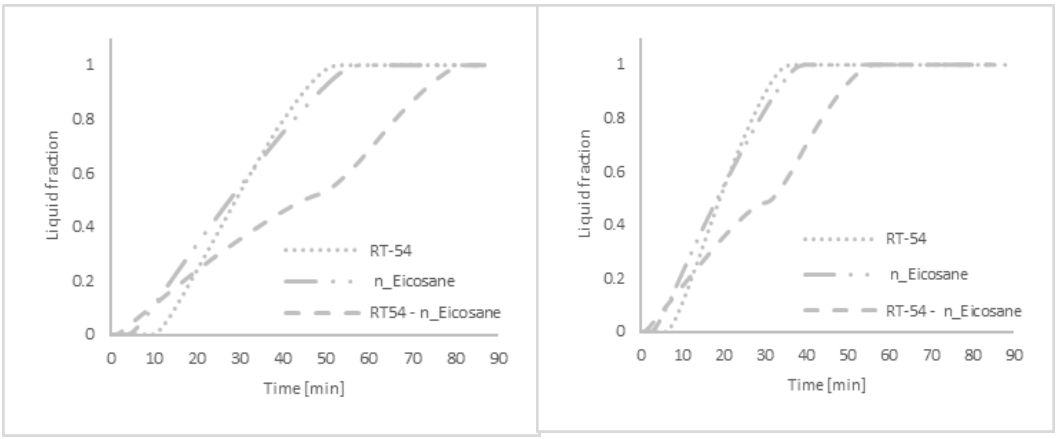

A) 5 B) 7.5

Fig.22: Changes in the volumetric fraction of liquid for the fourth scenario involving RT-54 and n–Eicosane at 5 and 7.5 W input powers.

For SPTs of 40, 45, and 55 degrees Celsius, the time required for the system temperature to attain the predetermined temperature varies across different materials and their combined scenario. At an SPT of 40 degrees Celsius, employing two materials concurrently at 5 W extends the time to reach the target temperature by 71% and at 7.5 W by 50% compared to the RT-54 case (Fig. 23-A). For an SPT of 45 degrees Celsius, the time extension is 100% at 5 W and 83% at 7.5 W (Fig.23-B). For an SPT of 55 degrees Celsius, the extension is 40% at 5 W and 44% at 7.5 W (Fig.23-C).

The lowest average temperature is observed in the n–Eicosane scenario, following which the combined scenario exhibits superior performance. As the input power rises, all cases' average system temperature elevates (Fig. 24).

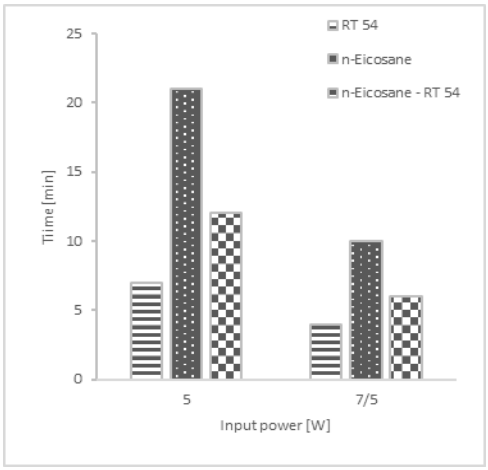

A) SPT 40

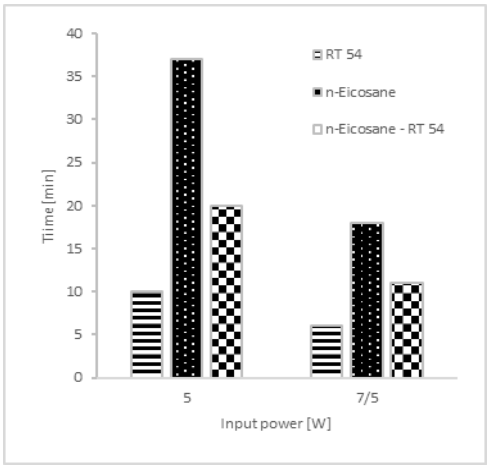

SPT 45

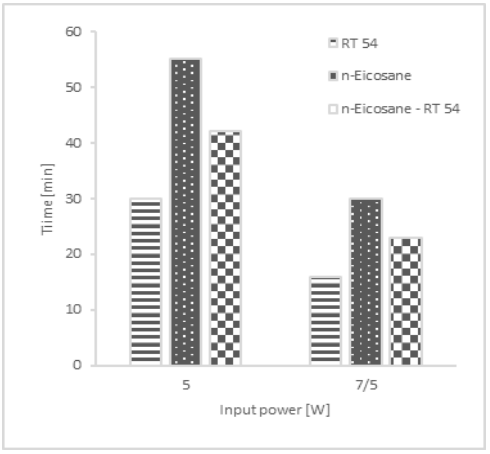

C) SPT 55

Fig.23: Set Point Temperature conditions for the fourth scenario involving RT-54 and n–Eicosane at 5 and 7.5 W input powers.

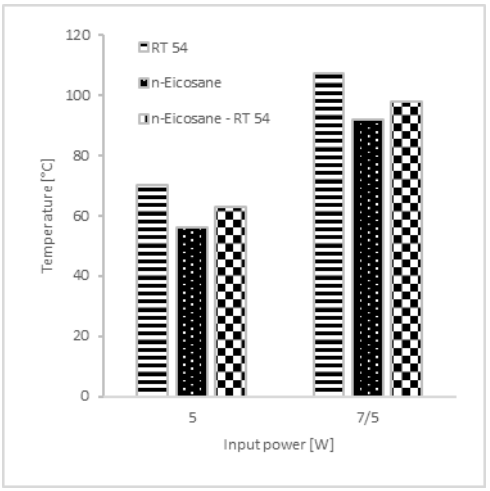

Fig.24: Average temperature of the thermal management system for the fourth scenario involving RT-54 and n–Eicosane at input powers of 5 and 7.5 W

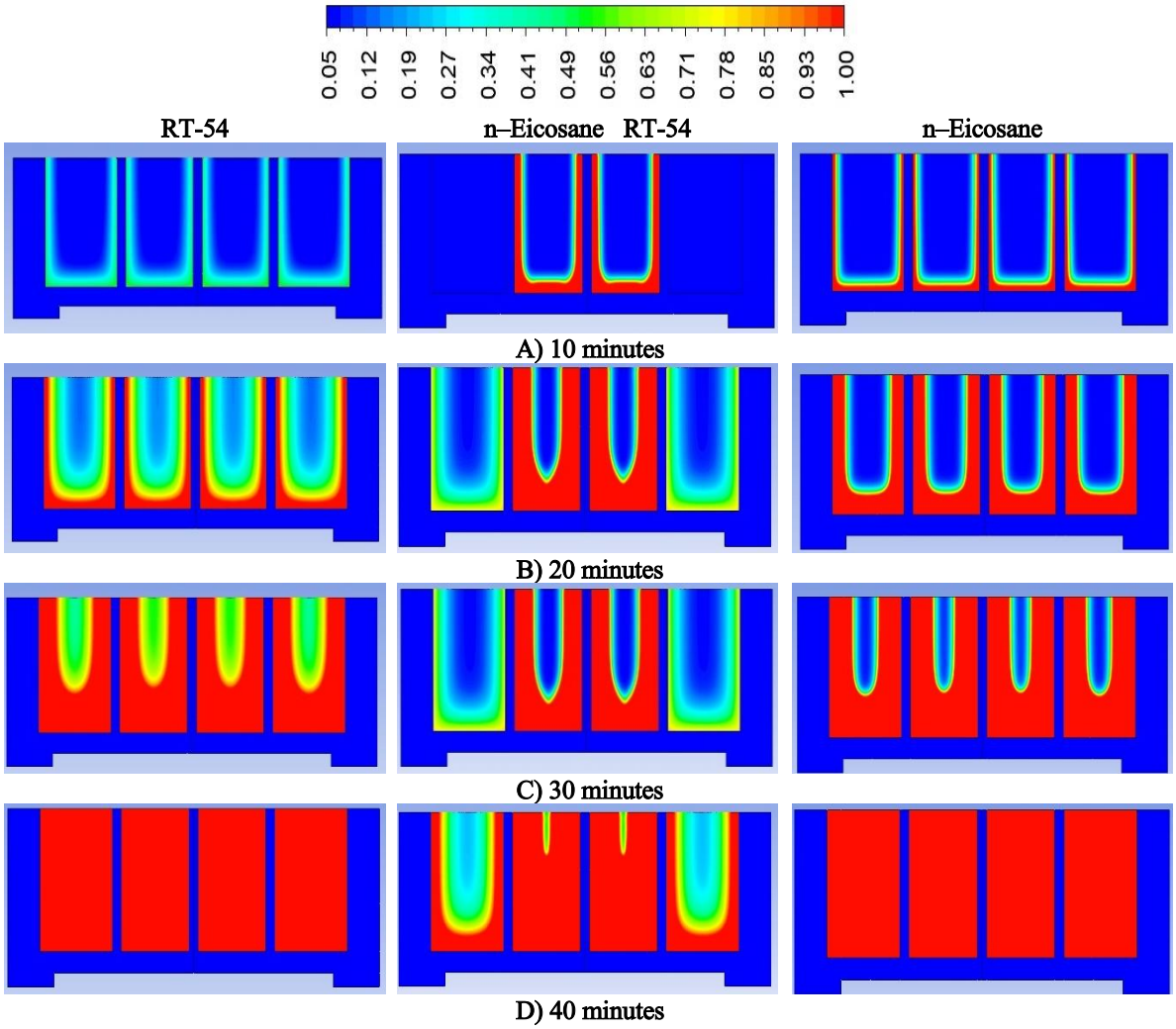

Fig.25: Volumetric fraction of liquid at different times for the fourth scenario involving RT-54 and n–Eicosane at an input power of 7.5 W.

7.Conclusion

This study investigated the implications of using multiple phase change materials (PCMs), both individually and in conjunction, within a two-dimensional heat sink at two distinct input power levels. The findings are summarized as follows:

- The density of the PCM plays a pivotal role in the outcomes. Despite its low latent heat of fusion, $CaCl_2.6H_2O$, due to its high density, necessitates more heat during phase transition. When considering PCMs separately, $CaCl_2.6H_2O$ yields the most favorable results. The latent heat of fusion of a material, which is the product of its mass and latent heat of fusion, should be considered when selecting a PCM.
- Given the passive nature of the system, the heat absorbed by the PCMs is the most crucial factor in maintaining the temperature stability of the thermal management system. Hence, in a material where the majority of the heat is consumed for the latent heat of fusion, the system resists temperature increases for a longer duration. This is conspicuously observed in using CaCl2.6H2O, followed by n–Eicosane and RT-54.
- Concurrent usage of two PCMs alters the operating conditions and, contingent upon the required melting heat, can enhance the system's thermal performance. Including $CaCl_2.6H_2O$ alongside the other two materials ameliorates their thermal performance metrics, such as Set Point

Temperature (SPT) and average system temperature.

- As the input power escalates, the impact of utilizing PCMs diminishes. This is attributed to the fact that, for all cases, an increase in input power leads to a decrease in SPT and a rise in the average system temperature.
- When two PCMs are used simultaneously, the thermal management system encounters two distinct melting points. One for the material with a lower melting temperature, and following the complete melting of the first material, the second material with a higher melting point commences its phase transition.
- Among the combined materials, $CaCl_2.6H_2O$, in conjunction with n–Eicosane, presents the greatest resistance against temperature change.
- During the melting of the PCM, a lower product of mass and latent heat of fusion corresponds to a decreased slope in temperature changes. This feature is particularly noticeable in the concurrent use of two materials, as depicted on the charts.
- Post complete melting of the PCMs, the slope of the temperature change curve is dependent on the specific heat of each material. A higher specific heat yields a lower slope in temperature changes.

References

[1] Bondareva, N.S. and M.A. Sheremet, Numerical study of PCMs arrangement effect on heat transfer performance in plate-finned heat sink for passive cooling system. Journal of Thermal Analysis and Calorimetry, 2022. 147(19): p. 10305-10317.

[2] Chu, Y.-M., S. Bilal, and M.R. Hajizadeh, Hybrid ferrofluid along with MWCNT for augmentation of thermal behavior of fluid during natural convection in a cavity. Mathematical Methods in the Applied Sciences, 2020. n/a(n/a).

[3] Mathew, V.K. and T.K. Hotta, Experimental investigation of substrate board orientation effect on the optimal distribution of IC chips under forced convection. Experimental Heat Transfer, 2021. 34(6): p. 564-585.

[4] 4. Shahsavar, A., et al., Numerical investigation of forced convection heat transfer and flow irreversibility in a novel heatsink with helical microchannels working with biologically synthesized water-silver nano-fluid. International Communications in Heat and Mass Transfer, 2019. 108: p. 104324.

[5] da Rosa, O.C., et al., Enhancing heat rejection from electronic devices with a supercritical carbon dioxide minichannel heat exchanger. International Journal of Refrigeration, 2019. 106: p. 463-473.

[6] Manova, S., et al., Cooling of high heat flux electronic devices using ultra-thin multiport minichannel thermosyphon. Applied Thermal Engineering, 2020. 169: p. 114669.

[7] Liu, X., Y. Chen, and M. Shi, Dynamic performance analysis on start-up of closed-loop pulsating heat pipes (CLPHPs). International Journal of Thermal Sciences, 2013. 65: p. 224-233.

[8] 8. Qu, J., et al., Recent advances in MEMS-based micro heat pipes. International Journal of Heat and Mass Transfer, 2017. 110: p. 294-313.

[9] Khalid, S.U., et al., Heat pipes: progress in thermal performance enhancement for microelectronics. Journal of Thermal Analysis and Calorimetry, 2021. 143(3): p. 2227-2243.

[10] Marri, G.K. and C. Balaji, Effect of phase change temperatures and orientation on the thermal performance of a miniaturized PCM heat sink coupled heat pipe. Experimental Heat Transfer, 2022: p. 1-23.

[11] Chen, A., et al., Experimental study on bubble characteristics of time periodic subcooled flow boiling in annular ducts due to wall heat flux oscillation. International Journal of Heat and Mass Transfer, 2020. 157: p. 119974.

[12] Yin, L., et al., Water flow boiling in a partially modified microgap with shortened micro pin fins. International Journal of Heat and Mass Transfer, 2020. 155: p. 119819.

[13] Malý, M., et al., Effect of nanoparticles concentration on the characteristics of nanofluid sprays for cooling applications. Journal of Thermal Analysis and Calorimetry, 2019. 135(6): p. 3375-3386.

[14] Zhao, J., et al., Thermal management strategy for electronic chips based on combination of a flat-plate heat pipe and spray cooling. International Journal of Heat and Mass Transfer, 2021. 181: p. 121894.
[15] Khan, U., et al., Radiative mixed convective flow induced by hybrid nanofluid over a porous vertical cylinder in a porous media with irregular heat sink/source. Case Studies in Thermal Engineering, 2022. 30: p. 101711.
[16] Shahsavar, A., et al., Hydrothermal and entropy generation specifications of a hybrid ferronanofluid in microchannel heat sink embedded in CPUs. Chinese Journal of Chemical Engineering, 2021. 32: p. 27-38.
[17] Ibrahim, M., et al., Energetic and exergetic analysis of a new circular micro-heat sink containing nanofluid: applicable for cooling electronic equipment. Journal of Thermal Analysis and Calorimetry, 2021. 145(3): p. 1547-1557.
[18] Alsarraf, J., et al., Numerical investigation on the effect of four constant temperature pipes on natural cooling of electronic heat sink by nanofluids: A multifunctional optimization. Advanced Powder Technology, 2020. 31(1): p. 416-432.
[19] Al-Rashed, A.A.A.A., et al., Numerical assessment into the hydrothermal and entropy generation characteristics of biological water-silver nano-fluid in a wavy walled microchannel heat sink. International Communications in Heat and Mass Transfer, 2019. 104: p. 118-126.
[20] Al-Rashed, A.A.A.A., et al., Numerical investigation of non-Newtonian water-CMC/CuO nanofluid flow in an offset strip-fin microchannel heat sink: Thermal performance and thermodynamic considerations. Applied Thermal Engineering, 2019. 155: p. 247-258.
[21] Khattak, Z. and H.M. Ali, Air cooled heat sink geometries subjected to forced flow: A critical review. International Journal of Heat and Mass Transfer, 2019. 130: p. 141-161.
[22] Ali, H.M., Recent advancements in PV cooling and efficiency enhancement integrating phase change materials based systems – A comprehensive review. Solar Energy, 2020. 197: p. 163-198.
[23] Muneeshwaran, M., et al., Performance improvement of photovoltaic modules via temperature homogeneity improvement. Energy, 2020. 203: p. 117816.
[24] Rostami, Z., et al., Enhancing the thermal performance of a photovoltaic panel using nano-graphite/paraffin composite as phase change material. Journal of Thermal Analysis and Calorimetry, 2022. 147(5): p. 3947-3964.
[25] Li, Z., et al., Numerical modeling of a hybrid PCM-based wall for energy usage reduction in the warmest and coldest months. Journal of Thermal Analysis and Calorimetry, 2021. 144(5): p. 1985-1998.
[26] Shahsavar, A., et al., Melting and solidification characteristics of a double-pipe latent heat storage system with sinusoidal wavy channels embedded in a porous medium. Energy, 2019. 171: p. 751-769.
[27] Shahsavar, A., et al., Numerical study of melting and solidification in a wavy double-pipe latent heat thermal energy storage system. Journal of Thermal Analysis and Calorimetry, 2020. 141(5): p. 1785-1799.
[28] Shahsavar, A., et al., Entropy and thermal performance analysis of PCM melting and solidification mechanisms in a wavy channel triplex-tube heat exchanger. Renewable Energy, 2021. 165: p. 52-72.
[29] Khalilmoghadam, P., A. Rajabi-Ghahnavieh, and M.B. Shafii, A novel energy storage system for latent heat recovery in solar still using phase change material and pulsating heat pipe. Renewable Energy, 2021. 163: p. 2115-2127.
[30] Wang, T., et al., Approaches for expedition of discharging of PCM involving nanoparticles and radial fins. Journal of Molecular Liquids, 2021. 329: p. 115052.
[31] Tariq, H.A., et al., Hydro-thermal performance of normal-channel facile heat sink using TiO2-H2O mixture (Rutile–Anatase) nanofluids for microprocessor cooling. Journal of Thermal Analysis and Calorimetry, 2021. 145(5): p. 2487-2502.
[32] Sriharan, G., S. Harikrishnan, and H. Ali, Experimental investigation on the

effectiveness of MHTHS using different metal oxide-based nanofluids. Journal of Thermal Analysis and Calorimetry, 2021. 143(2): p. 1251-1260.
[33] Li, F., et al., Melting process of nanoparticle enhanced PCM through storage cylinder incorporating fins. Powder Technology, 2021. 381: p. 551-560.
[34] Ghaneifar, M., et al., Mixed convection heat transfer of AL2O3 nanofluid in a horizontal channel subjected with two heat sources. Journal of Thermal Analysis and Calorimetry, 2021. 143(3): p. 2761-2774.
[35] Tariq, S.L., et al., Nanoparticles enhanced phase change materials (NePCMs)-A recent review. Applied Thermal Engineering, 2020. 176: p. 115305.
[36] Rashidi, S., et al., A review on potentials of coupling PCM storage modules to heat pipes and heat pumps. Journal of Thermal Analysis and Calorimetry, 2020. 140(4): p. 1655-1713.
[37] Ahmadlouydarab, M., M. Ebadolahzadeh, and H. Muhammad Ali, Effects of utilizing nanofluid as working fluid in a lab-scale designed FPSC to improve thermal absorption and efficiency. Physica A: Statistical Mechanics and its Applications, 2020. 540: p. 123109.
[38] Ahmadi, A.A., et al., Configuration and Optimization of a Minichannel Using Water–Alumina Nanofluid by Non-Dominated Sorting Genetic Algorithm and Response Surface Method. Nanomaterials, 2020. 10(5).
[39] Zhu, X., et al., Stable microencapsulated phase change materials with ultrahigh payload for efficient cooling of mobile electronic devices. Energy Conversion and Management, 2020. 223: p. 113478.
[40] Ho, J., et al., An experimental investigation of a PCM-based heat sink enhanced with a topology-optimized tree-like structure. Energy Conversion and Management, 2021. 245: p. 114608.
[41] Ren, Q., P. Guo, and J. Zhu, Thermal management of electronic devices using pin-fin based cascade microencapsulated PCM/expanded graphite composite. International Journal of Heat and Mass Transfer, 2020. 149: p. 119199.
[42] Kim, S.H., et al., Enhanced thermal performance of phase change material-integrated fin-type heat sinks for high power electronics cooling. International Journal of Heat and Mass Transfer, 2022. 184: p. 122257.
[43] Lamba, R., et al., PCM-based hybrid thermal management system for photovoltaic modules: A comparative analysis. Environmental Science and Pollution Research, 2023.
[44] Hu, X., et al., Thermal analysis and optimization of metal foam PCM-based heat sink for thermal management of electronic devices. Renewable Energy, 2023. 212: p. 227-237.
[45] Elshaer, A.M., et al., Boosting the thermal management performance of a PCM-based module using novel metallic pin fin geometries: Numerical study. Scientific Reports, 2023. 13(1): p. 10955.
[46] Balakrishnan, R., et al., Analysis of the thermal management of electronic equipment by employing silicon carbide nano-pcm-based heat sink. Environmental Science and Pollution Research, 2023.
[47] Tharwan, M.Y. and H.M. Hadidi, Experimental investigation on the thermal performance of a heat sink filled with PCM. Alexandria Engineering Journal, 2022. 61(9): p. 7045-7054.
[48] Sheikh, Y., M. Fatih Orhan, and M. Kanoglu, Heat transfer enhancement of a bio-based PCM/metal foam composite heat sink. Thermal Science and Engineering Progress, 2022. 36: p. 101536.
[49] Rehman, T.-u., et al., Experimental investigation on the performance of RT-44HC-nickel foam-based heat sinks for thermal management of electronic gadgets. International Journal of Heat and Mass Transfer, 2022. 188: p. 122591.
[50] Manoj Kumar, P., et al., Experimental analysis of a heat sink for electronic chipset cooling using a nano improved PCM (NIPCM). Materials Today: Proceedings, 2022. 56: p. 1527-1531.
[51] Mahmud, H. and D.H. Ahmed, Numerical Investigations on Melting of Phase Change Material (PCM) with Different Arrangements of Heat Source-sink

Pairs Under Microgravity. Microgravity Science and Technology, 2022. 34(2): p. 20.
[52] Kim, J., et al., Enhanced thermal performances of PCM heat sinks enabled by layer-by-layer-assembled carbon nanotube–polyethylenimine functional interfaces. Energy Conversion and Management, 2022. 266: p. 115853.
[53] Jalil, J.M., H.S. Mahdi, and A.S. Allawy, Cooling performance investigation of PCM integrated into heat sink with nano particles addition. Journal of Energy Storage, 2022. 55: p. 105466.
[54] Al-Omari, S.A.B., et al., Thermal management characteristics of a counter-intuitive finned heat sink incorporating detached fins impregnated with a high thermal conductivity-low melting point PCM. International Journal of Thermal Sciences, 2022. 175: p. 107396.
[55] Ali, H.M., An experimental study for thermal management using hybrid heat sinks based on organic phase change material, copper foam and heat pipe. Journal of Energy Storage, 2022. 53: p. 105185.
[56] Wang, S., et al., Experimental study on the thermal performance of PCMs based heat sink using higher alcohol/graphite foam. Applied Thermal Engineering, 2021. 198: p. 117452.
[57] Sunku Prasad, J., R. Anandalakshmi, and P. Muthukumar, Numerical investigation on conventional and PCM heat sinks under constant and variable heat flux conditions. Clean Technologies and Environmental Policy, 2021. 23(4): p. 1105-1120.
[58] Hu, X. and X. Gong, Experimental study on the thermal response of PCM-based heat sink using structured porous material fabricated by 3D printing. Case Studies in Thermal Engineering, 2021. 24: p. 100844.
[59] Ho, J.Y., et al., An experimental investigation of a PCM-based heat sink enhanced with a topology-optimized tree-like structure. Energy Conversion and Management, 2021. 245: p. 114608.
[60] Dammak, K. and A. El Hami, Thermal reliability-based design optimization using Kriging model of PCM based pin fin heat sink. International Journal of Heat and Mass Transfer, 2021. 166: p. 120745.
[61] Taghilou, M. and E. Khavasi, Thermal behavior of a PCM filled heat sink: The contrast between ambient heat convection and heat thermal storage. Applied Thermal Engineering, 2020. 174: p. 115273.
[62] Motahar, S. and M. Jahangiri, Transient heat transfer analysis of a phase change material heat sink using experimental data and artificial neural network. Applied Thermal Engineering, 2020. 167: p. 114817.
[63] Gaddala, U.M. and J.K. Devanuri, A Hybrid Decision-Making Method for the Selection of a Phase Change Material for Thermal Energy Storage. Journal of Thermal Science and Engineering Applications, 2020. 12(4).
[64] Debich, B., et al., Design optimization of PCM-based finned heat sinks for mechatronic components: A numerical investigation and parametric study. Journal of Energy Storage, 2020. 32: p. 101960.
[65] Akula, R. and C. Balaji, Thermal Performance of a Phase Change Material-Based Heat Sink Subject to Constant and Power Surge Heat Loads: A Numerical Study. Journal of Thermal Science and Engineering Applications, 2020. 13(3).
[66] Kalbasi, R., et al., Studies on optimum fins number in PCM-based heat sinks. Energy, 2019. 171: p. 1088-1099.
[67] Usman, H., et al., An experimental study of PCM based finned and un-finned heat sinks for passive cooling of electronics. Heat and Mass Transfer, 2018. 54(12): p. 3587-3598.
[68] Arshad, A., et al., An experimental study of enhanced heat sinks for thermal management using n-eicosane as phase change material. Applied Thermal Engineering, 2018. 132: p. 52-66.
[69] Arıcı, M., et al., Investigation on the melting process of phase change material in a square cavity with a single fin attached at the center of the heated wall★. Eur. Phys. J. Appl. Phys., 2018. 83(1): p. 10902.
[70] Ali, H.M., et al., Thermal management of electronics devices with PCMs filled pin-fin heat sinks: A comparison. International Journal of Heat and Mass Transfer, 2018. 117: p. 1199-1204.
[71] Arshad, A., et al., Thermal performance of phase change material (PCM) based pin-

finned heat sinks for electronics devices: Effect of pin thickness and PCM volume fraction. Applied Thermal Engineering, 2017. 112: p. 143-155.

[72] Ali, H.M., et al., Thermal management of electronics: An experimental analysis of triangular, rectangular and circular pin-fin heat sinks for various PCMs. International Journal of Heat and Mass Transfer, 2018. 123: p. 272-284.

[73] Ashraf, M.J., et al., Experimental passive electronics cooling: Parametric investigation of pin-fin geometries and efficient phase change materials. International Journal of Heat and Mass Transfer, 2017. 115: p. 251-263.

[74] Brent, A.D., V.R. Voller, and K.J. Reid, ENTHALPY-POROSITY TECHNIQUE FOR MODELING CONVECTION-DIFFUSION PHASE CHANGE: APPLICATION TO THE MELTING OF A PURE METAL. Numerical Heat Transfer, 1988. 13(3): p. 297-318.

[75] Yang, Y.-T. and Y.-H. Wang, Numerical simulation of three-dimensional transient cooling application on a portable electronic device using phase change material. International Journal of Thermal Sciences, 2012. 51: p. 155-162.

[76] Wang, Y.-H. and Y.-T. Yang, Three-dimensional transient cooling simulations of a portable electronic device using PCM (phase change materials) in multi-fin heat sink. Energy, 2011. 36(8): p. 5214-5224.

[77] Shatikian, V., G. Ziskind, and R. Letan, Numerical investigation of a PCM-based heat sink with internal fins: Constant heat flux. International Journal of Heat and Mass Transfer, 2008. 51(5): p. 1488-1493.

[78] Nayak, K.C., et al., A numerical model for heat sinks with phase change materials and thermal conductivity enhancers. Int. J. Heat Mass Transf, 2006. vol. 49(null): p. 1833.

[79] Shatikian, V., G. Ziskind, and R. Letan, Numerical investigation of a PCM-based heat sink with internal fins. Int. J. Heat Mass Transf, 2005. vol. 48(null): p. 3689.

[80] Sahoo, S.K., P. Rath, and M.K. Das, Numerical study of phase change material based orthotropic heat sink for thermal management of electronics components. International Journal of Heat and Mass Transfer, 2016. 103: p. 855-867.

[81] Hosseinizadeh, S., F. Tan, and S. Moosania, Experimental and numerical studies on performance of PCM-based heat sink with different configurations of internal fins. Appl. Therm. Eng., 2011. 31(17–18): p. 3827.

[82] Fok, S.C., W. Shen, and F.L. Tan, Cooling of portable hand-held electronic devices using phase change materials in finned heat sinks. Int. J. Thermal Sci, 2010. vol. 49(null): p. 109.

[83] Hosseini, M.J., M. Rahimi, and R. Bahrampoury, Experimental and computational evolution of a shell and tube heat exchanger as a PCM thermal storage system. International Communications in Heat and Mass Transfer, 2014. 50: p. 128-136.

[84] Kumar, A., et al., Experimental investigation on paraffin wax-based heat sinks with cross plate fin arrangement for cooling of electronic components. Journal of Thermal Analysis and Calorimetry, 2022. 147(17): p. 9487-9504.